CHAPTER 6

ROLE OF THERMAL TREATMENTS PRE- AND POST- ULTRASONIC SHOT PEENING ON LCF BEHAVIOR

6.1 Introduction

Low cycle fatigue (LCF) behavior of the AA7075 was studied in three different conditions: (i) peak aged-ultrasonic shot peened (PA-USSP), (ii) peak aged-ultrasonic shot peened and stress relieved (PA-USSP-SR) and (iii) solution treated-ultrasonic shot peened-peak aged (ST-USSP-PA), at room temperature. The un-shot peened samples are designated as PA-unUSSP. The peak aged samples subjected to USSP are designated as PA-USSP. The USSP treatment was carried out for 180 seconds at a constant amplitude of 80 μm with hard steel balls of 3 mm diameter. Following the USSP treatment, some samples were subjected to stress relieving treatment at 90°C for 4 h to relieve the residual stress and these samples are designated as PA-USSP-SR. Another set of the specimens of the as-received material was subjected to solution treatment at 470°C for 30 min to dissolve the precipitates formed in the peak aged condition and these specimens were subjected to USSP for the same duration of 180 seconds and subsequently to peak aging (PA). These are designated as ST-USSP-PA. LCF tests were conducted under fully reversed axial strain control at total strain amplitudes from ±0.38% to ±0.60%. Fatigue life was found to be highest for the ST-USSP-PA among the three conditions referred to above. In all the

three conditions comparable nanostructures were developed up to the depth of $\sim$ 50 μm, however, the size of the strengthening precipitates was relatively large ($\sim$ 20nm) in the ST-USSP-PA in comparison with those in the other two conditions ($\sim$ 7-8 nm). High resolution TEM examination revealed high density of dislocations in the matrix and also within precipitates in the PA-USSP, however, dislocations were not observed in precipitates in the other two conditions. The high fatigue life in the ST-USSP-PA condition is attributed to more homogeneous distribution, larger size and higher volume fraction of the strengthening precipitates of η', in delaying the process of crack initiation.

6.2 Microstructure

In depth microstructural characterization of the un-USSP sample has already been discussed in the previous chapter in section 3.2.2. The microstructure modification in the PA-USSP, PA-USSP-SR and ST-USSP-PA conditions are explained in subsequent sections. Fig. 6.1a shows microstructure of the USSP treated sample with equiaxed nanograins; the corresponding selected area diffraction pattern (SADP) in the inset shows formation of ring pattern confirming the presence of nano sized grains. There was no effect of USSP on the fine GP-zone and η' precipitates; these were homogeneously distributed throughout the matrix (Fig. 6.1b). However, most of the coarse precipitates of η (Fig. 6.1c) and E-phase (Fig. 6.1d) were fragmented and got reduced in size due to the repeated impact of hard steel balls from USSP treatment. The size and density of these precipitates is shown in Table 6.1. There was also generation of high density of dislocations ($\sim$ 4x10^{16} m^{-2}),

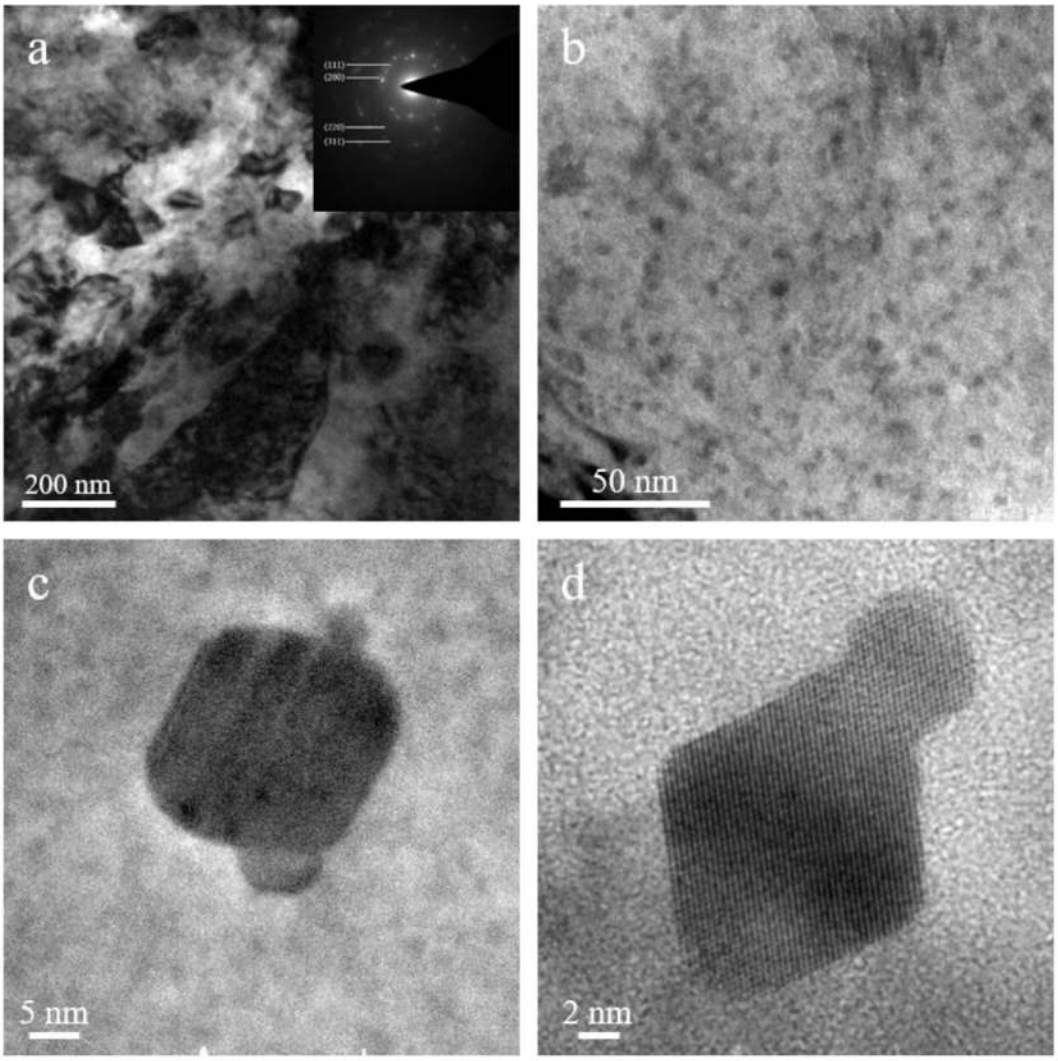

FIGURE 6.1: Bright field TEM micrograph of the AA7075: (a) PA-USSP condition with its corresponding SADP, (b) GP-zones and η' precipitates, (c) HRTEM of η-phase and (d) HRTEM of E-phase.

arranged in tangled configuration, due to severe plastic deformation caused by the USSP treatment.

The SADP of the stress relieved sample shows that the grains were in the nanometer range even after the stress relieving treatment following the USSP treatment (Fig. 6.2a). It is evident from the TEM micrograph that there is considerable decrease in the dislocation density due to the stress relieving treatment. The boundaries of the grains were found to

be non-blurry which is a characteristic feature of a strain free miscrostructure suggesting some relieving of strain on thermal exposure.

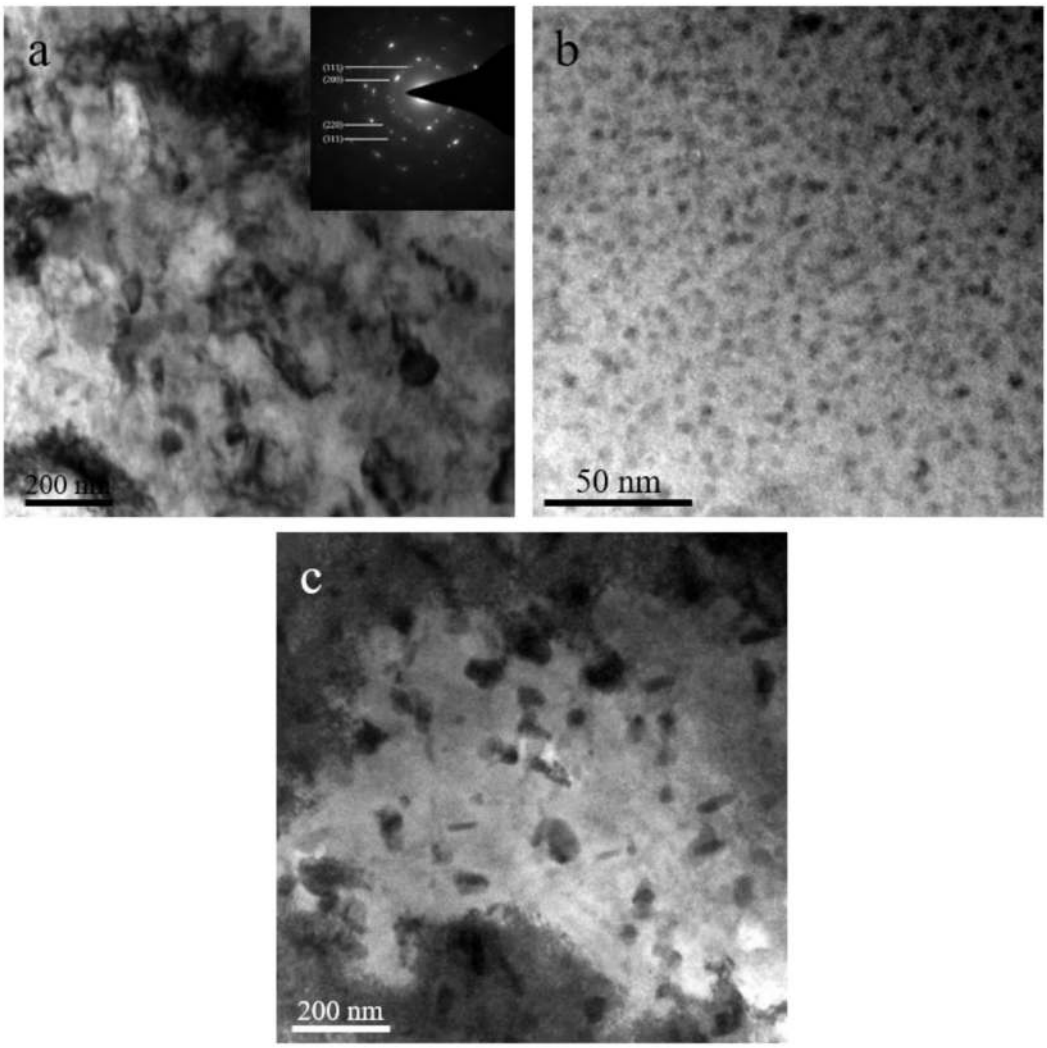

FIGURE 6.2: Bright field TEM micrograph of the AA7075: (a) PA-USSP-SR condition with its corresponding SADP, (b) GP-zones and η' precipitates, and (c) showing coarse η and E-phase precipitates.

Fig. 6.2b shows homogeneously distributed GP-zones and η' precipitates throughout the matrix. The number density of these precipitates was found to increase, however, there was no effect on the overall volume fraction as compared to that of the USSP treated specimen. The unaffected coarse precipitates of η and E (Fig. 6.2c) from the USSP treatment

TABLE 6.1: Microstructural Characteristics of the AA7075 in different conditions.

Treatment condition	**Precipitate type**	**Average size (nm)**	**Dislocation density (m^{-2})**
PA-unUSSP	GP-zone	5	5.5941 x10^{15}
	η'	10	
	η	85	
PA-USSP	GP-zone	5	3.7675x10^{16}
	η'	10	
	η	42	
PA-USSP-SR	GP-zone	5	5.9612x10^{15}
	η'	10	
	η	80	
ST-USSP-PA	GP-zone	8	9.2146x10^{15}
	η'	10	
	η	80	

were observed to be coarsened ($\sim$ 80 nm) following the thermal exposure.

In the ST-USSP-PA condition there is more homogeneous distribution of the strengthening precipitates. The discontinuous ring in the SADP inset (Fig. 6.3a) signifies presence of nanograined structure even after the peak aging treatment. The microstructure after the aging treatment shows clusters of very fine platelets (Fig. 6.3b), the typical round clusters are GP-zones and the fine platelets are of η' precipitates. The η' precipitates with average size of 5.1 nm x 23.8 nm were distributed homogeneously throughout the matrix and oriented in a particular direction and the density of these precipitates was found to be higher as compared to the other treated conditions. An HRTEM of an individual precipitate of η' is shown in Fig. 6.3c and the FFT in the inset shows that these precipitates are aligned parallel to (100) planes. The precipitation was especially around the dislocation substructure, generated by the USSP treatment, because of nucleation of the precipitates preferentially at the dislocations.

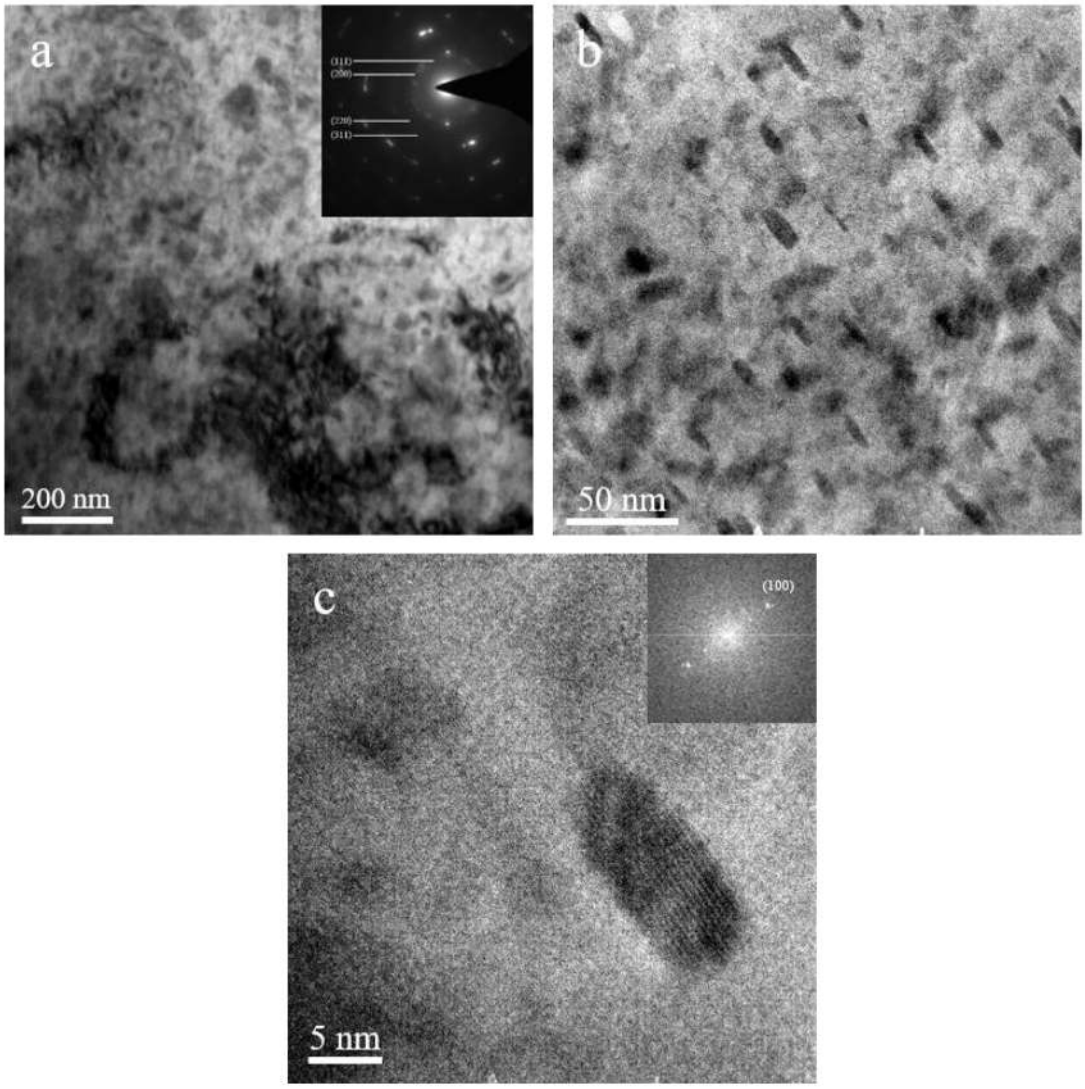

FIGURE 6.3: Bright field TEM micrograph of the AA7075: (a) ST-USSP-PA condition with its corresponding SADP, (b) GP-zones, η' precipitates and (c) HRTEM of η' precipitates.

6.3 Tensile Properties

The engineering stress-strain curves of the AA7075 in the different conditions are shown in Fig. 6.4 and the tensile properties are recorded in the Table 6.2. While there is decrease in the yield strength (S_y) and tensile strength (S_u) due to the stress relieving treatment (PA-USSP-SR), there is increase in both of these parameters in the ST-USSP-PA condition.

TABLE 6.2: Tensile properties of the AA7075 in different conditions.

Treatment Condition	YS (MPa)	UTS (MPa)	e_u (%)	e_f(%)	S_u/S_y
PA-USSP	321	518	7.40	9.10	1.61
PA-USSP-SR	281	498	7.50	8.90	1.77
ST-USSP-PA	336	548	7.90	10.20	1.63

The uniform strain as well as the strain to fracture are highest for the ST-USSP-PA and the degree of work hardening is highest for the PA-USSP-SR condition.

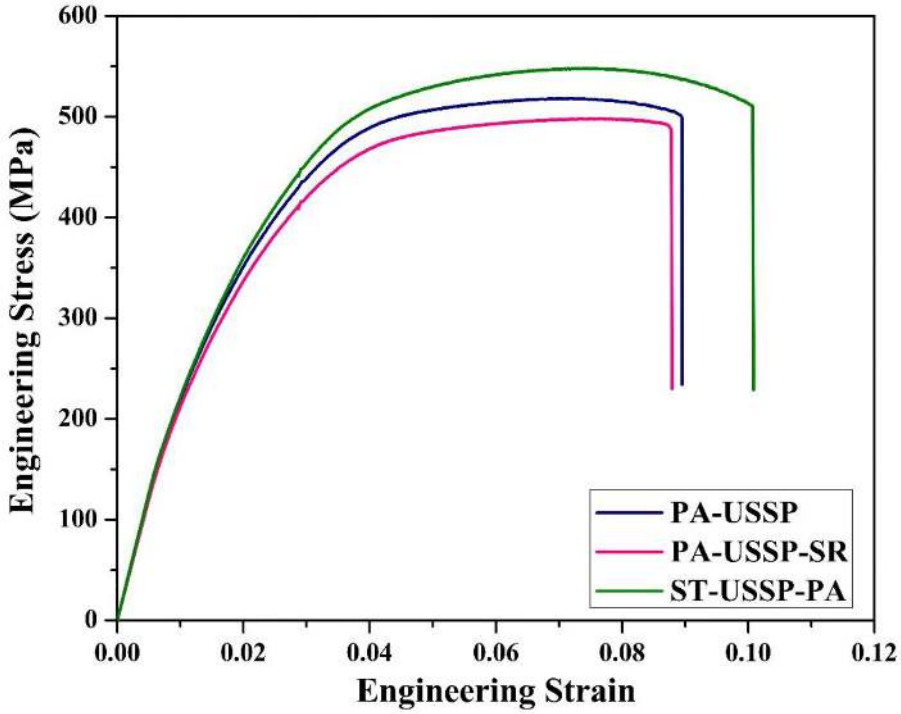

FIGURE 6.4: Engineering stress-strain curves of the AA7075 in different conditions.

6.4 Low Cycle Fatigue Behavior

Fig. 6.5 shows cyclic stress response curves of the AA7075 in the PA-USSP, PA-USSP-SR and ST-USSP-PA conditions at different total strain amplitudes. The cyclic stress response

of the USSP treated (USSP 180) specimen has already been discussed in the Chapter-5. Cyclic hardening was observed for the PA-USSP-SR during the initial 100 cycles, followed by stabilization of the cyclic stress. The degree of cyclic hardening increased with increase in the strain amplitude. In the ST-USSP-PA samples initial cyclic hardening was observed only at the higher strain amplitudes ($\geq \pm 0.45\%$), on the other hand there was a stable stress response at the lower stain amplitudes, till the failure. Cyclic hardening was relatively more in the PA-USSP-SR as compared with that in the ST-USSP-PA condition.

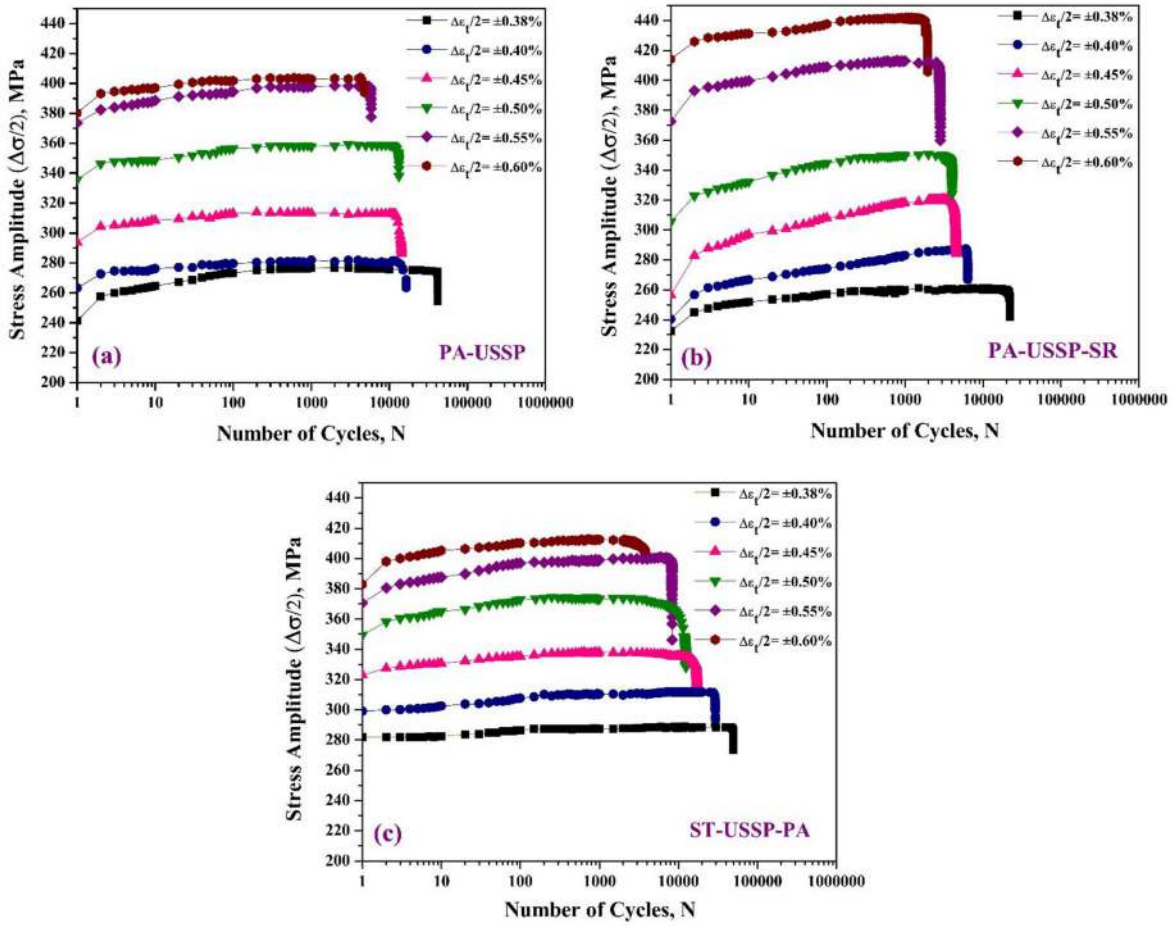

FIGURE 6.5: Cyclic stress response curves of the AA7075 in different conditions (a) PA-USSP, (b) PA-USSP-SR and (c) ST-USSP-PA.

Coffin–Manson relationship, between the plastic strain amplitude ($\Delta\epsilon_p/2$) and the

TABLE 6.3: LCF parameters obtained from the Coffin-Manson plot.

Treatment Condition	ϵ'_f	c
PA-USSP	0.0027	-0.37
PA-USSP-SR	0.0025	-0.36
ST-USSP-PA	0.0002	-0.09

number of reversals to failure ($2N_f$) was used to analyze the fatigue life in different conditions, as given below.

$$\Delta\epsilon_p/2 = \epsilon'_f(2N_f)^c \tag{6.1}$$

where ϵ'_f and c are fatigue ductility coefficient and exponent, respectively. The Coffin-Manson plots for the different conditions are shown in Fig. 6.6. The LCF parameters obtained from the plots in Fig. 6.6 are presented in Table 6.3. It may be seen that in the ST-USSP-PA condition the values of ϵ'_f and c are the lowest and fatigue life is the highest.

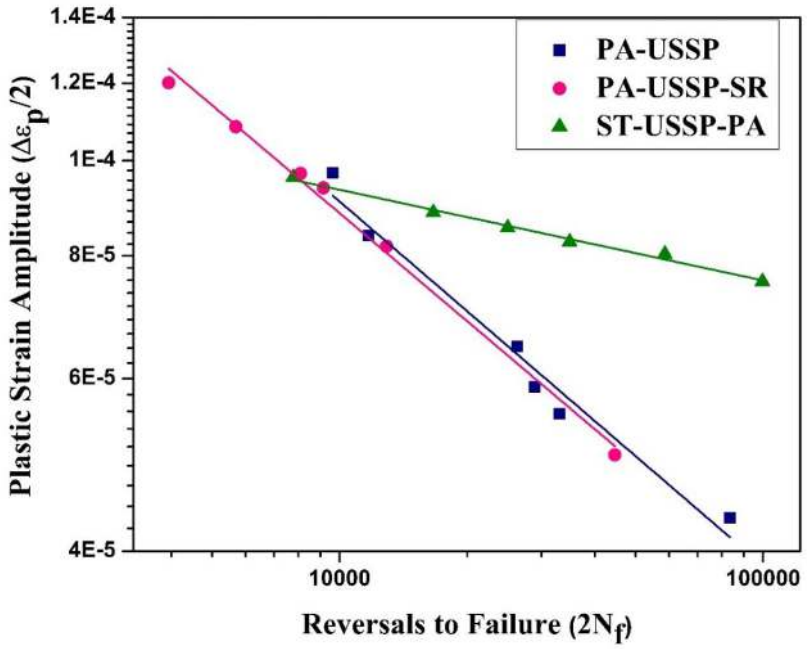

FIGURE 6.6: Dependence of fatigue life, as reversals to failure, on plastic strain amplitude.

The variation of the number of cycles to failure at different total strain amplitudes for the different conditions is shown in Fig. 6.7. After the stress relieving treatment of the USSP treated specimen, the LCF life is reduced, on the other hand fatigue life is increased in the ST-USSP-PA condition and is the highest amongst the three conditions.

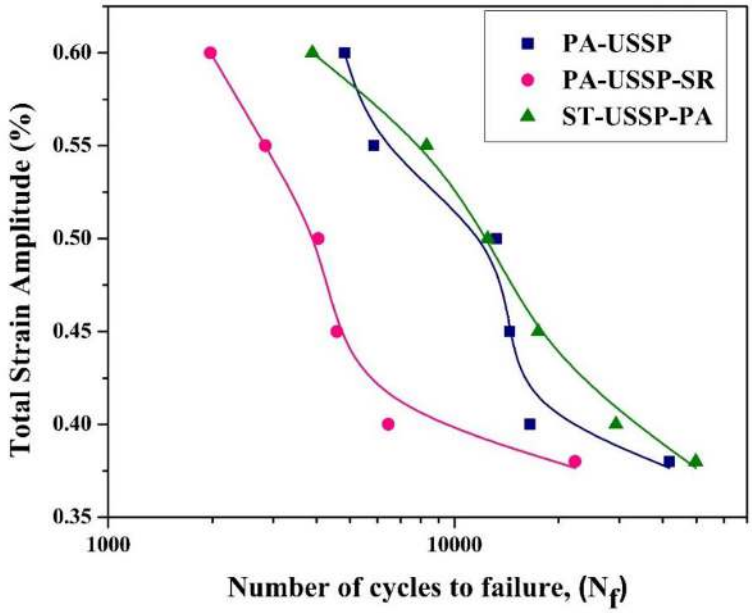

FIGURE 6.7: Dependence of fatigue life on total strain amplitude for different conditions.

The high fatigue life in the ST-USSP-PA condition in respect of the other two conditions (Fig. 6.6 & Fig. 6.7) may be analyzed from Fig. 6.8 which shows the variation of the two components of fatigue life, N_i and N_p. It may be seen from Fig. 6.8 that both N_i and N_p for the ST-USSP-PA are more or less comparable to the other two conditions, at the highest strain amplitude of ±0.60%; however, at the lower strain amplitudes from ±0.55% to ±0.38%, N_i is significantly enhanced for the ST-USSP-PA in comparison with those of the other two conditions. Further, the difference between the N_i and N_p increases markedly with decrease in the strain amplitude. On the other hand, there is not much

difference in N_p for the three conditions. Thus, it is obvious that the high fatigue life in the ST-USSP-PA condition is essentially due to high resistance of the material in this condition against fatigue crack initiation.

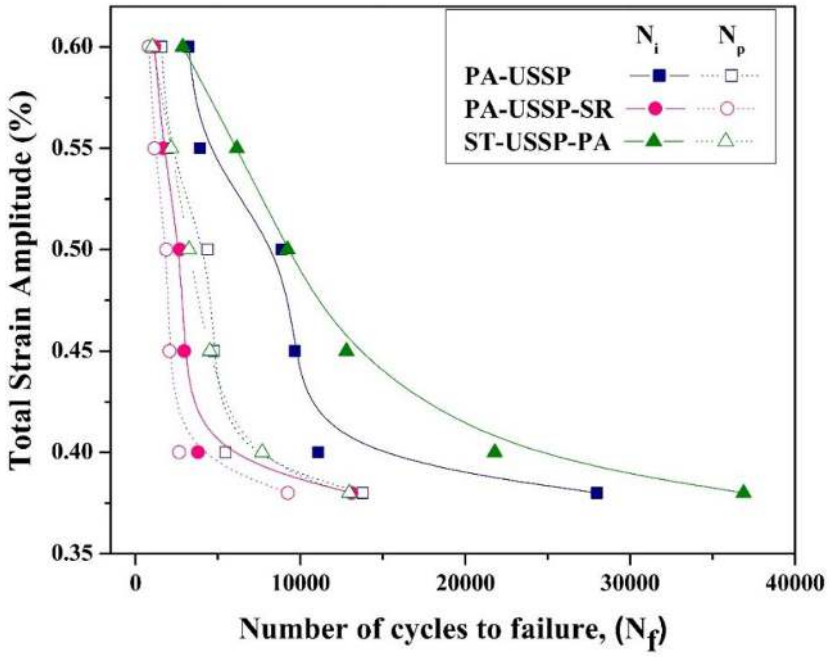

FIGURE 6.8: Variation of the number of cycles for crack initiation (N_i) and for crack propagation (N_p) for the AA7075 tested in LCF at different total strain amplitudes.

The fractured surfaces of the samples tested at the intermediate strain amplitude of $\Delta\epsilon_t/2$=±0.45% for the above three conditions are shown in Fig. 6.9. Fatigue cracks may be seen to initiate from the surface (marked with yellow arrows) in all the conditions and no sub-surface crack initiation was there. The number of crack initiation sites is more in the USSP treated specimen (Fig. 6.9a). The mode of crack propagation is transgranular and the direction of fatigue crack growth (FCG) is shown by the arrows in Fig. 6.9a', b', c'. An approximation was made for the rate of crack propagation calculating the interstriation spacings in Stage-II crack propagation. The interstriation spacings calculated from the fractographs of the PA-USSP, PA-USSP-SR and ST-USSP-PA are found to be 0.75, 1.21

and 0.63 μm/cycle respectively. Thus, it is also obvious from these data that the rate of crack propagation was the lowest in the ST-USSP-PA condition.

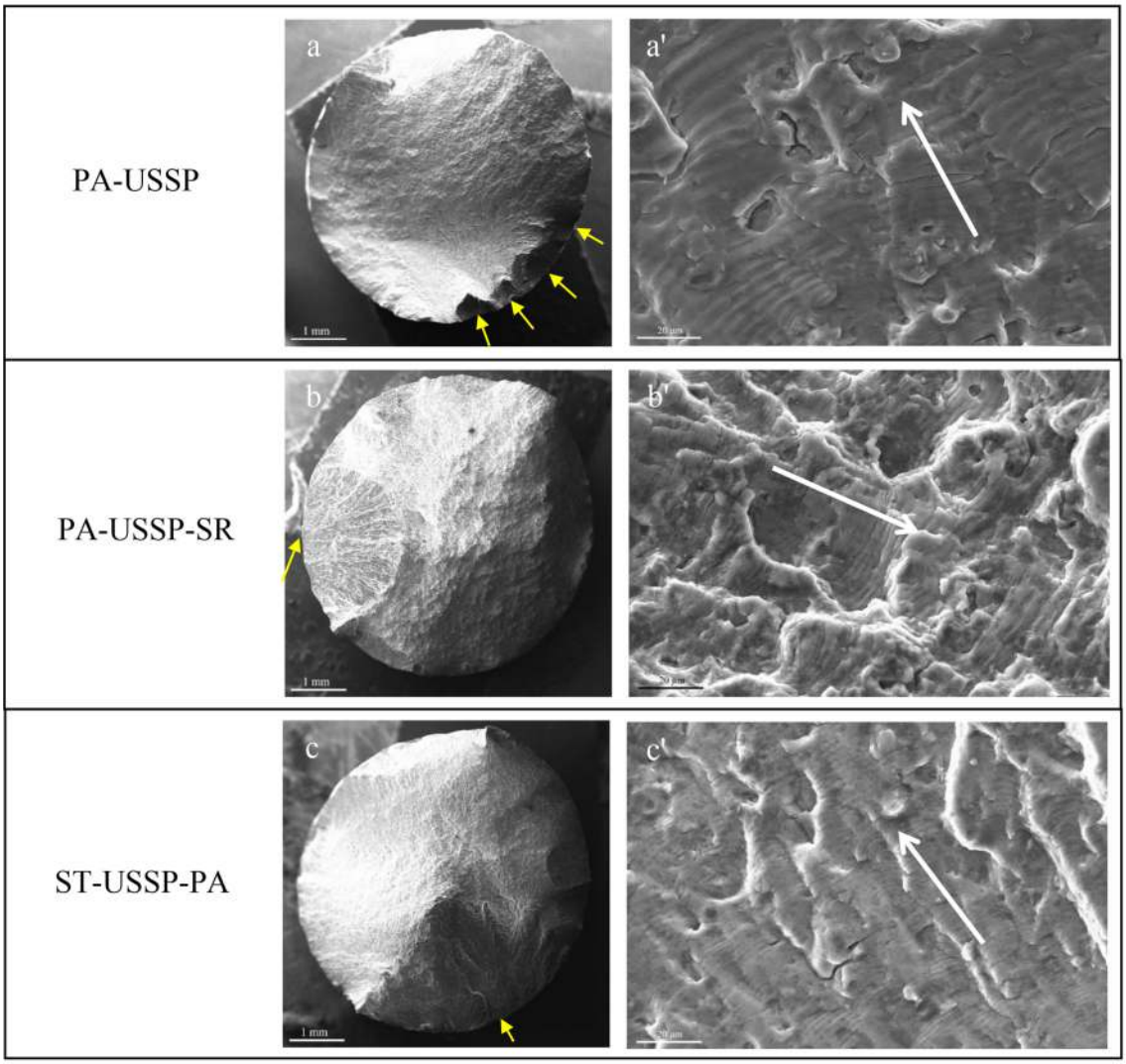

FIGURE 6.9: SEM fractographs showing overall fracture surfaces and fatigue striation in the specimens tested at the total strain amplitude of ±0.45%: (a) PA-USSP, (b) PA-USSP-SR and (c) ST-USSP-PA.

6.5 Discussion

As mentioned in the introduction, the present investigation was undertaken to study the effect of pre and post USSP thermal treatment for lowering the residual compressive stress and modify the microstructure by USSP treatment, thermal treatments and modifying the size and distribution of strengthening precipitates. In all the three conditions: PA-USSP, PA-USSP-SR and ST-USSP-PA, the USSP treatment was identical for 180 seconds with shots of 3 mm diameter. However, the initial condition of the AA7075 was peak aged for the PA-USSP and PA-USSP-SR, whereas it was solution treated for the ST-USSP-PA. Further, while no thermal treatment was given to PA-USSP, stress relieving treatment was given to PA-USSP and it was designated as PA-USSP-SR, whereas peak age hardening treatment was given to ST-USSP and it was designated as ST-USSP-PA.

As mentioned earlier, ultrasonic shot peening led to development of nanostructure in surface region of the specimens, in all the three conditions as established by XRD and TEM analysis. The original coarse-grains were refined to nano-scale due to severe plastic deformation of the surface region from repeated multidirectional impacts of hard steel balls. It is evident from the characteristic ring-shaped SAD pattern of the shot peened surface region that an extremely fine-grained structure developed with high angles of misorientation. Along with the nanosized grains some η and E particles were also present in the PA-USSP-SR condition, distributed heterogeneously in the matrix. Further, there was no change in the size of surface grains following the stress relieving treatment, however, there was recovery and the dislocation density was reduced, with increase in the size of the precipitates (Fig. 6.2).

There was decrease in volume fraction of the precipitates, in particular of the coarse ones, due to the USSP treatment, suggesting their fragmentation and dissolution in the matrix, in line with the earlier observation made by Krishna et.al in the ultrafine grained Al–4Zn–2Mg alloy produced by cryorolling [73]. The stress relieving treatment led to increase in the size and volume fraction of the coarse precipitates of η as compared to that of the PA-USSP condition. However, there was no effect on the fine precipitates of η' (Fig. 6.2b). On the other hand, in the ST-USSP-PA condition volume fraction of the coarse precipitates was low and the fine precipitates were relatively larger in size with more uniform distribution than that in the initial peak aged condition (Fig. 6.3b). It is due to high density of dislocations produced by USSP of the solution treated specimen, to act as nucleation sites for the precipitates. The size of the strengthening precipitates was relatively larger ($\sim$ 23 nm) in the ST-USSP-PA condition in comparison with those in the PA-USSP and in PA-USSP-SR conditions ($\sim$7-8 nm). Large number of grain boundaries in the nanostructured surface region enhanced the rate of diffusion and the kinetics of precipitation to result in more homogeneous distribution of the strengthening precipitates [73].

The HRTEM micrographs and their corresponding inverse fast Fourier transform (IFFT) images for the different conditions are shown in Fig. 6.10. The density of dislocations in the USSP treated condition was estimated to be 3.7675x10^{16} m^{-2} and most of the dislocations were observed to surround the second phase η particles (Fig. 6.10a$'$). These dislocations of high density were not able to pass/glide the precipitates and increased the hardness in the USSP treated regime. At high strain when the dislocations were able to

pass through the precipitates it led to fragmentation of the precipitates. The high density of dislocations, generated during the USSP treatment was drastically reduced to 5.9612x10^{15} m^{-2} in the stress relieved condition due to recovery.

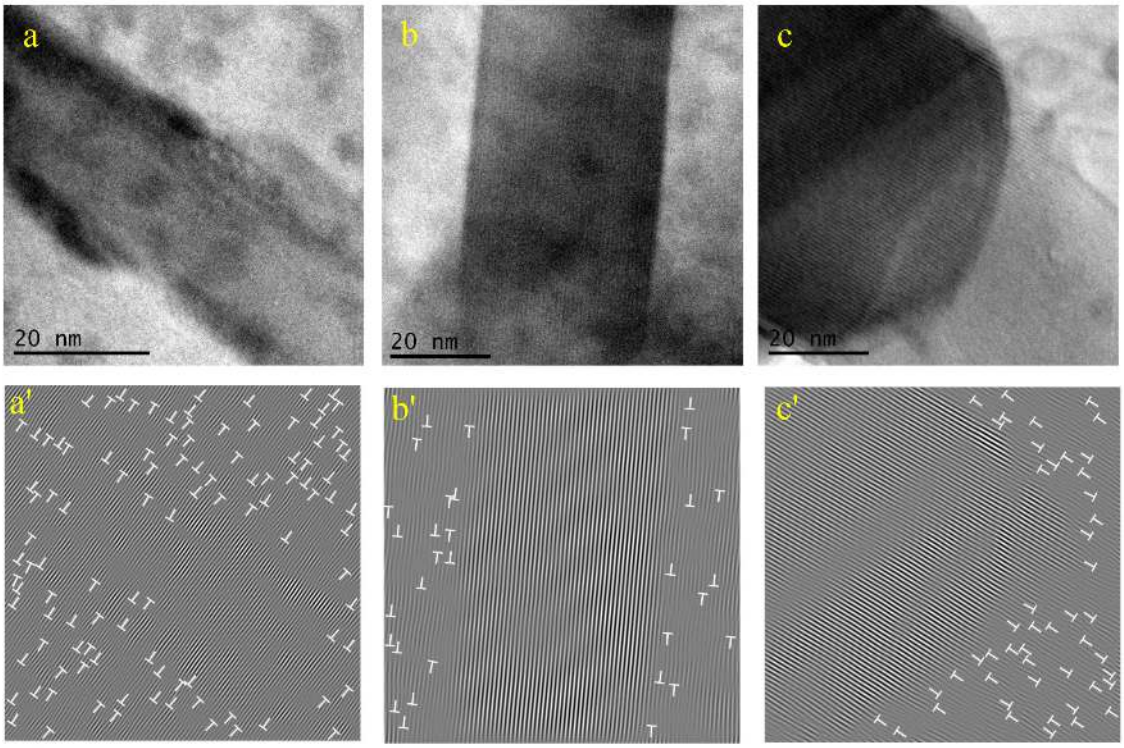

FIGURE 6.10: HRTEM micrographs and corresponding IFFT images of dislocation distribution around precipitates in (a) PA-USSP, (b) PA-USSP-SR and (c) ST-USSP-PA.

The decrease in dislocation density and partial relieving of the compressive residual stress caused decrease in hardness in the surface region. The increase in grain boundary fraction resulting from USSP enhanced the rate of diffusion and consequently the formation of nano precipitates which retarded the mobility of dislocations and caused strengthening of the AA7075 [91]. These nanosized precipitates compensated for the fall in the dislocation density (9.2146x10^{15} m^{-2}) and also the fall in the compressive residual stress, thus the overall strength of the AA7075 was enhanced. These observations are in

line with those of Cheng et.al [90] who reported that there were smaller precipitates in the AA2024 due to cryo-rolling and subsequent aging, and also their density was high to cause strengthening.

The high strength and elongation in the ST-USSP-PA condition was mainly due to high density of fine precipitates of the metastable η'. Zhao et. al [88] also observed enhanced tensile strength in the AA7075 in solutionized, cryo-rolled and peak aged condition which was attributed to improved work hardening rate.The low dislocation density, following peak aging treatment of the ST-USSP treated specimen left much room for dislocation accumulation before saturation, increased the degree and rate of work-hardening.The high density of nanosize precipitates was effective in pinning and accumulation of dislocations to increase the work-hardening rate [90].

There is considerable difference in cyclic stress response of the alloy in the three conditions (Fig. 6.5). It may be seen that there is significant increase in the stress amplitude in the second cycle itself in the PA-USSP and PA-USSP-SR and the increase is relatively more in the PA-USSP-SR than that in PA-USSP. Further, the cyclic stress amplitude rises progressively up to about 100 cycles in the PA-USSP and thereafter remains constant till before the fracture (Fig. 6.5a), whereas the stress amplitudes continuously increases up to nearly 2000 cycles before stabilization in the PA-USSP-SR (Fig. 6.5b). Also, the degree of work hardening is higher in the PA-USSP-SR as compared with that in the PA-USSP, at almost all the strain amplitudes from ±0.38% to ±0.60%. The relatively higher stress amplitude in the first cycle in the case of PA-USSP at the lower strain amplitudes from ±0.38% to ±0.45% in respect of that of the PA-USSP-SR is due to initial high density of

dislocations in the PA-USSP condition. The relatively lower cyclic stress amplitude at the first cycle of PA-USSP than that of PA-USSP-SR at the high strain amplitudes from ±0.50% to ±0.60% is due to the effect of the precipitates formed during the stress relieving treatment of the PA specimen following the USSP treatment. The degree of cyclic work hardening is the highest in the PA-USSP-SR among the three conditions and it is due to initial low density of dislocations resulting from the stress relieving treatment coupled with precipitation of fine precipitates from the stress relieving treatment.

The cyclic stress response in the ST-USSP-PA is quite different from those of PA-USSP and PA-USSP-SR. The stress amplitude of the first cycle is relatively higher for the ST-USSP-PA than those of the PA-USSP as well as PA-USSP-SR at the lowest strain amplitudes of ±0.38% and ±0.40% and it remains nearly unchanged up to the first ten cycles. There is slight increase in the cyclic stress amplitude in the second cycle at the higher strain amplitude of ±0.45% and it progressively increases at the higher strain amplitudes. There is relatively less tendency of work hardening than in the PA-USSP-SR condition, however it is relatively higher than that in the PA-USSP and lower than that in PA-USSP-SR. The typical cyclic stress response of ST-USSP-PA in respect of the other two conditions may be attributed to stronger precipitates in the ST-USSP-PA and the interaction of dislocations with precipitates.

Nanostructuring in surface region has been reported to delay the process of fatigue crack initiation and the high compressive residual stresses associated with the gradient microstructure in the sub-surface region to retard the process of fatigue crack propagation [137, 142]. It may be noted that, in general, the number of cycles for crack initiation

(N_i) is higher than the number of cycles to crack propagation (N_p). In the ST-USSP-PA condition there is large difference between the N_i and N_p and the difference between N_i and N_p progressively increased with decrease in the total strain amplitude. N_i may be seen to increase rapidly at the lower strain amplitudes of ±0.40% and more so at ±0.38%. It is due to the presence of the strengthening precipitates in the nanostructured surface layer, which made dislocation movements more difficult under the applied fatigue stress, due to which the process of fatigue crack nucleation was delayed and N_i increased (Fig. 6.8).

Ductile materials perform better under strain controlled low cycle fatigue (LCF) and majority of the fatigue life is spent in the process of fatigue crack propagation, whereas, strong materials show better resistance under stress controlled high cycle fatigue (HCF) where large fraction of fatigue life is spent in the process of fatigue crack initiation. Therefore, surface nanostructuring induced by USSP treatment is more effective at the lower strain amplitudes as compared with that at the higher strain amplitudes which is obvious from Fig. 6.7. Nanostructured surface layer displays higher yield strength as per the Hall-Petch relationship, whereas the strain hardening increases the mechanical strength through dislocation entanglement, thus further permanent deformation is delayed [143]. Grain refinement causes shortening of slip distance due to which the level of stress concentration is reduced and the resistance against fatigue crack initiation is improved and thus fatigue life is enhanced [142]. Also, compressive residual stress plays a significant role in improving the ductility by suppressing cracking in the surface and sub-surface region. In Fig. 3.18 residual stress remains compressive up to a depth of $\sim$ 250 μm from the surface. This makes the affected region hard and the un-affected coarse grained region

soft and a large strain gradient is developed under loading due to gradient residual stress which promotes further accumulation of dislocations and produces extra strain hardening and thereby crack propagation is also arrested to some extent [91].

Thus, the enhancement of LCF life in the ST-USSP-PA condition is due to homogeneous precipitation of extremely fine GP-zones and η' precipitates. The decrease in dislocation density and fall in the residual stress was compensated by relatively larger size of the strengthening precipitates ($\sim$ 24 nm). LCF life of the PA-USSP-SR specimens was found to be less as compared to that of the PA-USSP condition. It can be seen from Fig. 6.8 that the difference between N_i and N_p was very low which indicates that relieving of compressive residual stress from the surface region (Fig. 3.18) results in decrease of both N_i and N_p and consequently LCF life was decreased. Stress relieving treatment did not alter the microstructure in the surface region, the grains were of nano size and there was no grain growth. In the AA2014 the stress relieving treatment resulted in increase of LCF life and it was attributed to complete removal of the tensile residual stress generated from the USSP treatment in the sub-surface region, however, an opposite trend was observed in the alloy Ti-6Al-4V [61, 144].

6.6 Conclusions

The following conclusions are drawn from this chapter:

1. The high density of dislocations generated during USSP promoted nanosize precipitates of second phase particles during the peak aging treatment.

2. In ST-USSP-PA condition the high density of η' precipitates along with nanograined surface layer resulted in delaying the process of crack initiation and thus LCF life was enhanced.

3. Pinning of dislocations due to precipitates led to increase in the ductility and simultaneous increment in LCF properties.

4. Decrease in dislocation density and relieving of compressive residual stress was observed after the stress relieving treatment which resulted in decrease in the LCF life.